IEEE Access
Multidisciplinary : Rapid Review : Open Access Journal

Received January 22, 2019, accepted February 17, 2019, date of publication February 26, 2019, date of current version March 13, 2019.

Digital Object Identifier 10.1109/ACCESS.2019.2901846

Effects of Temperature and Residual Stresses on the Output Characteristics of a Piezoresistive Pressure Sensor

ANH VANG TRAN[1,2], XIANMIN ZHANG[1], AND BENLIANG ZHU[1]

[1]Guangdong Key Laboratory of Precision Equipment and Manufacturing Technology, School of Mechanical and Automotive Engineering, South China University of Technology, Guangzhou 510640, China
[2]Faculty of Aerospace Engineering, Le Quy Don Technical University, Hanoi 100000, Vietnam

Corresponding author: Benliang Zhu (meblzhu@scut.edu.cn)

This work was supported by the National Natural Science Foundation of China under Grant 51605166 and Grant 51820105007.

ABSTRACT The effects of temperature on the output performance of piezoresistive pressure sensors are studied in this paper. The influences of the environmental temperature, the residual stress due to the fabrication process, and the residual stress due to the packaging on the piezoresistive coefficient and resistance are theoretically investigated. The simulation results are obtained via finite element analysis through ANSYS. The results of experimental studies performed on piezoresistive pressure sensors fabricated using MEMS techniques are reported to verify the simulation results. The output characteristics of piezoresistive pressure sensors are shown to be substantially affected by not only the environmental temperature but also the residual stresses from the fabrication and packing processes.

INDEX TERMS MEMS, pressure sensor, piezoresistive devices, thermal drift.

I. INTRODUCTION

Mems pressure sensors provide the ability to measure the low-pressure range and have the advantages of small size, low power requirements, good performance and the ability to be mass produced via micromachining [1]. Pressure sensors are among the most widely used MEMS products on the market. Notably, these sensors have a variety of applications, such as in microscale mechatronic systems [2], automobiles [3], aerodynamics [4], [5], process control [6] and biomedical equipment [7], [8]. On the basis of their sensing principles, MEMS pressure sensors can be divided into piezoresistive, capacitive, optical, and resonance sensors, among other types. Piezoresistive pressure sensors are the most frequently applied type because they have significant advantages over other sensors, such as good linearity, high pressure sensitivity, small size, high performance, low cost, and easy fabrication [9]. A piezoresistive pressure sensor consists of a diaphragm and four piezoresistors in a Wheatstone bridge configuration. The diaphragm is subjected to pressure loading, transforming the input pressure into a stress field [10], [11]. In pressure sensor applications, the devices often operate in variable-temperature environments. Unfortunately, the main disadvantage of piezoresistive sensors is the effect of temperature on the sensor output, which leads to thermal zero shift and sensitivity drift. Moreover, these pressure sensors are often fabricated and packaged under high-temperature conditions. Therefore, thermal residual stress influences the measurement results of piezoresistive sensors [12]. Numerous studies have been conducted to evaluate this limitation to improve the sensor performance. The contributing factors can be classified into three main categories: the effects of temperature on the piezoresistive coefficient and resistance, the thermal residual stress due to the fabrication process, and the residual stress due to the sensor chip packaging.

First, the effects of the doping level on the thermal behavior of silicon resistors have been studied, and the results show that the thermal coefficients of the resistors and the piezoresistive coefficient are functions of the doping level and temperature [13]. The thermal variations of the offset voltages of piezoresistive pressure sensors have also determined under the assumption of piezoresistors with different thermal coefficients [14]. In other reports, various theoretical and experimental methods have been adopted to estimate the thermal drift characteristics of piezoresistive

The associate editor coordinating the review of this manuscript and approving it for publication was Hamid Mohammad-Sedighi.

2169-3536 © 2019 IEEE. Translations and content mining are permitted for academic research only.
Personal use is also permitted, but republication/redistribution requires IEEE permission.
See http://www.ieee.org/publications_standards/publications/rights/index.html for more information.

pressure sensors. In these studies, the dependences of the piezoresistive coefficient and zero-offset voltage on the temperature and temperature drift were considered [15]. Unfortunately, the thermal residual stresses on the sensor diaphragm were not considered when estimating the thermal effects.

Second, the thermal residual stress generated during the fabrication of sensor chips influences thermal hysteresis [16]. For example, Chiou and Chen [17] reported a thermal hysteresis analysis of MEMS pressure sensors in which it was found that different layouts and areas of the metal pads led to different residual stresses on the resistors. The same results were found by Hsin-Nan Chiang. Experimental and simulation results showed that the dimensions and placement of the aluminum traces influenced the hysteresis voltage [18]. Clearly, these studies overlooked a key component: the thermal behavior of silicon resistors was not considered. In addition, the sensor chips were fabricated by cutting a single chip from a silicon wafer after a series of fabrication processes, so the residual stress in the silicon wafer due to the passivation layers deposited on the silicon substrate should be considered.

Third, the purpose of sensor packaging is to enhance the sensor sensitivity and reduce thermal effects by means of silicone gel [12]. Krondorfer *et al.* [19] studied the effect of epoxy-based molding compound packaging on MEMS pressure sensors and found that the stresses induced by the molding compound influenced the sensor output. Additionally, Chiou [20] compared two types of packaging with a glass substrate to isolate the thermal stress from the plastic housing, which substantially reduced the thermal hysteresis. While many studies have addressed the thermal behavior of piezoresistors and the residual stresses in the membrane originating from the fabrication process, the causes of thermal instability remain important concerns in pressure sensor design and fabrication. Therefore, considerable attention has been paid to determining the causes of temperature effects in silicon pressure sensors.

In this paper, the influences of the environmental temperature, the residual stress due to the fabrication process, and the residual stress due to the packaging on the piezoresistive coefficient and resistance are investigated. A theoretical model has been developed to study the thermal behavior of piezoresistors. The thermal residual stresses of sensor chips are analyzed by means of finite element analysis (FEA) using ANSYS software. The results of multiple experiments conducted on piezoresistive pressure sensors fabricated via MEMS techniques are reported to verify the simulation results and the performance of the sensors.

II. EXPERIMENTAL PIEZORESISTIVE PRESSURE SENSOR DESIGN

A piezoresistive pressure sensor design has been developed to validate the instability of the thermal performance of such sensors. The design method and sensor chip fabrication process have previously been studied by Tran *et al.* [21]. The dimensions are shown in a three-quarter section view in Figure 1. The sensor die is designed from a silicon wafer.

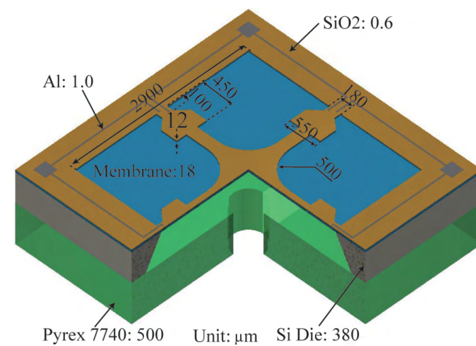

FIGURE 1. Model of the proposed sensor chip.

The structure consists of a novel combined crossbeam-peninsula structure on the membrane to generate higher stresses on the piezoresistor locations. Four piezoresistors are placed on top in a Wheatstone bridge configuration. SiO_2 is used as a passivation layer to prevent the elements from being damaged during the fabrication process. Pyrex 7740 glass is anodically bonded to the sensor die. Bulk micromachining technology is applied to fabricate a sensor chip from a standard n-type (100) silicon wafer of 380 μm in thickness. The MEMS techniques of low-pressure chemical vapor deposition (LPCVD) photolithography, anisotropic dry etching and boron implantation are employed to form the sensing elements and p-type silicon piezoresistors.

A. THE SENSING PRINCIPLE

The sensor design is based on piezoresistive effects, which can change a physical signal into an electrical signal. Generally, a piezoresistive sensor includes four resistors, which are placed on the stress concentration regions and arranged in a Wheatstone bridge configuration with two longitudinal piezoresistors (R_1 and R_3) and two transverse piezoresistors (R_2 and R_4). Briefly, it is assumed that the diaphragm is designed on n-type silicon, with all resistors being of p-type silicon with their longer axes along the (110) direction (Figure 2). In the initial state, $R_1 = R_2 = R_3 = R_4 = R_0$, and the resistance change ΔR_i very small relative to R_0. On the basis of the Wheatstone bridge circuit, the equation relating the output voltage V_o and the input voltage V_{in} can be expressed as [22]

$$\begin{aligned} V_{out} &= \frac{1}{4}\left(\frac{\Delta R_1}{R_1} - \frac{\Delta R_2}{R_2} + \frac{\Delta R_3}{R_3} - \frac{\Delta R_4}{R_4}\right) V_{in} \\ &= \frac{1}{2}\left(\frac{\Delta R_1}{R_1} - \frac{\Delta R_2}{R_2}\right) V_{in}. \end{aligned} \quad (1)$$

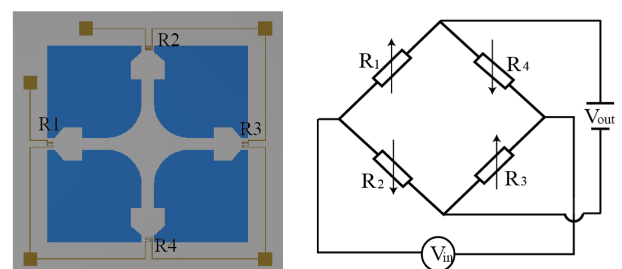

FIGURE 2. Wheatstone bridge.

Clearly, the output performance of a piezoresistive sensor depends on the resistance variation. Therefore, any fluctuations in resistance lead to device performance instability, especially when the sensor is operating in an environment of variable temperature and pressure. Generally, when such a sensor is subjected to variable stresses and temperatures, the piezoresistance of the silicon material ($\Delta R/R$) will change. Suppose that the average longitudinal stress of a resistor is σ_l and that the average transverse stress is σ_t. The fractional change in resistance can be written as a combination of the longitudinal and transverse components:

$$\frac{\Delta R}{R} = \pi_l \sigma_l + \pi_t \sigma_t, \tag{2}$$

where π_l and π_t are the longitudinal and transverse piezoresistive coefficients, respectively, and σ_l and σ_t are the longitudinal and transverse stresses, respectively. For p-silicon piezoresistors oriented in the $< 110 >$ direction on a (100) silicon wafer, Eq. (2) can be rewritten as follows:

$$\frac{\Delta R}{R} = \frac{\pi_{44}}{2} (\sigma_l - \sigma_t,) \tag{3}$$

where π_{44} is the shearing piezoresistance coefficient. By inserting Eq. (3) into Eq. (1), the sensor output voltage can be expressed as

$$\begin{aligned} V_{out} &= \frac{1}{2}\left[\frac{1}{2}\pi_{44}(\sigma_l - \sigma_t) - \frac{1}{2}\pi_{44}(\sigma_t - \sigma_l)\right] V_{in} \\ &= \frac{1}{2}\pi_{44}(\sigma_l - \sigma_t) V_{in}. \end{aligned} \tag{4}$$

Equation (4) expresses how the piezoresistance coefficient and stresses affect the voltage output of the sensor. The piezoresistance coefficient is sensitive to the temperature, doping level, conductivity type and orientation of the resistors. Meanwhile, the stresses on the sensor can depend on the operating pressure and temperature. The thermal stresses due to the fabrication process and packaging that are caused by thermal mismatch must also be considered in this study.

B. THERMAL PERFORMANCE INSTABILITY

In the proposed sensor, several materials with different thermal expansion coefficients are combined into one unit. The fabrication process is also conducted under different temperature conditions. Thus, the thermal performance instability is considered to originate from three main sources: the temperature dependence of the piezoresistive coefficient and resistances, the residual stress in the deposited thin-film layers, and the residual stress due to the adhesion of the Pyrex 7740 glass to the sensor chip (see Figure 3).

1) In the first set of steps, boron ions are implanted on part of each crossbeam peninsula to form the piezoresistors. The resulting piezoresistive coefficient is a function of the doping level and temperature.
2) In the second set of steps, thin films of 0.6 μm SiO_2 and 1.0 μm aluminum are deposited via LPCVD to protect the sensor surface and create the electrical connection lines of the Wheatstone bridge.

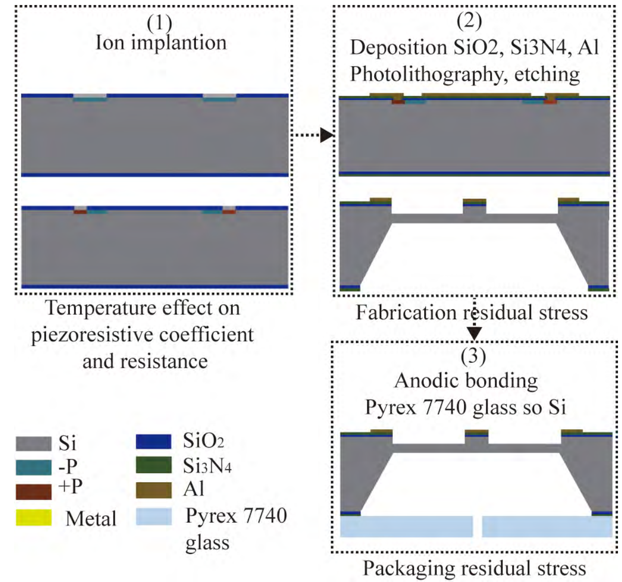

FIGURE 3. Prediction of the thermal performance instability of the sensor due to the fabrication process and packaging.

3) Finally, the back side of the sensor chip is attached to Pyrex 7740 glass at 300 to 600 °C. The fabrication process and packaging are the main sources of residual stress on the sensor membrane.

III. THERMAL PERFORMANCE INSTABILITY OF THE PIEZORESISTIVE PRESSURE SENSOR

A. EFFECTS OF TEMPERATURE ON THE PIEZORESISTIVE COEFFICIENT AND RESISTANCES

When the pressure loading applied to the diaphragm is zero and the four piezoresistors are fully matched, the sensor output voltage must be equal to zero. However, temperature variations can change the values of the resistors; therefore, the offset voltage of the sensor will change. The influence of temperature on the piezoresistor behavior is described as follows [14]:

$$R_i(T) = R_i^0(1 + \alpha_i \Delta T + \beta_i \Delta T^2), \tag{5}$$

where i is the number of the piezoresistive element ($i = 1, 2, 3, 4$), ΔT is the difference between the reference temperature T_0 and the operating temperature (the reference temperature is usually 200 °C), $R_i(T)$ is the conductor resistance at temperature T, R_{0i} is the conductor resistance at the reference temperature, and α_i and β_i are the temperature coefficients of resistance (TCR).

The Wheatstone bridge in Figure 2 is divided into two parts: the left and right half-bridges. The left half-bridge includes resistors R_1 and R_2. For this half-bridge, the output voltage at temperature T is given by

$$\frac{V_{o12}(T)}{V_{in}} = \frac{R_1(T)}{R_1(T) + R_2(T)}. \tag{6}$$

The variation in the offset voltage of the left half-bridge at temperature T is given by

$$\frac{\Delta V_{o12}(T)}{V_{in}} = \frac{R_1^0}{R_1^0 + R_2^0} - \frac{R_1(T)}{R_1(T) + R_2(T)} = \frac{R_1^0 R_2^0}{(R_1^0+R_2^0)^2}\left[(\alpha_1-\alpha_2)\,\Delta T + (\beta_1 - \beta_2)\,\Delta T^2\right]. \tag{7}$$

The resulting thermal variation in the zero-offset voltage can be written as

$$\frac{V_{offset}(T)}{V_{in}} = \frac{R_1^0 R_2^0}{(R_1^0 + R_2^0)^2}\left[(\alpha_1 - \alpha_2)\,\Delta T + (\beta_1 - \beta_2)\,\Delta T^2\right] - \frac{R_3^0 R_4^0}{(R_3^0+R_4^0)^2}\left[(\alpha_3-\alpha_4)\,\Delta T+(\beta_3-\beta_4)\,\Delta T^2\right]. \tag{8}$$

In the initial state, $R_1 = R_2 = R_3 = R_4 = R_0$, and the resistance change ΔR_i is small relative to R_0. The zero-offset voltage induced by TCR can be written as

$$\frac{V_{offset}(T)}{V_{in}} = \frac{1}{4}\sum_{1}^{4}(-1)^{i+1}\left[(\alpha_i)\,\Delta T + (\beta_i)\,\Delta T^2\right]. \tag{9}$$

Moreover, the piezoresistance coefficient is a function of the doping level and temperature of the p-type silicon. This function is denoted by $\pi_{44}(N, T)$, where N is the doping level and T is the temperature, and is expressed as follows [20], [23]:

$$\pi_{44}\,(N, T) = \pi_{44}(N_0, 300\text{ K})P(N, T), \tag{10}$$

where $\pi_{44}(N_0, 300\text{ K})$ is the piezoresistance coefficient at room temperature. In this study, consideration is given to the temperature features as well as the sensitivity. The ion implantation concentration is set to $3 \times 10^{-18}\text{ cm}^{-3}$, so $\pi_{44}(N_0, 300\text{ K})$ is $138.1 \times 10^{-11}\text{ Pa}^{-1}$. $P(N, T)$ is the piezoresistance factor, which depends on the doping level and temperature and is determined by the following equation:

$$P(N, T) = \frac{300}{T}\,\frac{1}{\left(1 + \exp\left(-\frac{E_f}{K_b T}\right)\right)\ln\left(1 + \exp\left(\frac{E_f}{K_b T}\right)\right)}, \tag{11}$$

where E_f is the Fermi energy of the doped silicon and K_b is the Boltzmann constant. The piezoresistance factor $P(N, T)$ and the piezoresistance coefficient $\pi(N, T)$ are functions of the doping level and temperature of the p-type silicon. For an operating temperature of T and a stress of σ on the sensor, the output voltage of the full bridge in (4) can be written as follows:

$$\frac{V_{out}(T)}{V_{in}} = V_{offset}(T) + \frac{1}{2}\pi_{44}(N_0, 300K)P(N, T)\,(\sigma_l - \sigma_t). \tag{12}$$

The first term in (12) is the output voltage induced by TCR, and the second is the effect of the temperature on the piezoresistive coefficient.

B. RESIDUAL STRESS DUE TO THE FABRICATION PROCESS

As mentioned above, the piezoresistive pressure sensor consists of a diaphragm and four piezoresistors. The resistors are placed on top of the membrane in high-stress regions to maximize the piezoresistive effect. Therefore, the sensor performance is strongly influenced by the stresses on the resistors. In addition to the stresses induced by pressure loading, residual stress, often arising from the fabrication process, plays an important role in the thermal hysteresis of the sensor. The sensor membrane is an important component: residual stress often arises during its preparation. As discussed in the third section, this residual stress is mainly induced by the deposition of the SiO_2 and Al passivation layers via LPCVD. Residual stress is defined as the stress remaining in a material and includes three components: thermal, intrinsic and quenching stresses [24]. Hsueh *et al.* [25] studied the residual stress in a multilayer system consisting of n thin layers, each of thickness t_i, bonded sequentially to a substrate of thickness t_s. In this case, the substrate is much thicker than the film layers. After the multilayer system is subjected to a temperature change of ΔT, the residual stresses in the thin films (σ_i^R) and in the substrate (σ_s^R) can be calculated as follows:

$$\sigma_s^R = \frac{2(3z + 2t_s)}{t_s^2}\sum_{i=1}^{n} E_i' t_i(\alpha_i - \alpha_s)\Delta T, \tag{13}$$

$$\sigma_i^R = E_i'(\alpha_i - \alpha_s)\Delta T, \tag{14}$$

where $E' = E/(1 - \nu)$ is the biaxial modulus; E and ν are the Young's modulus and Poisson's ratio, respectively; and α_i and α_s are the coefficients of thermal expansion (CTEs) of the thin films and the substrate, respectively. When the sensor is subjected to a variable stress, the stress on the sensor membrane can been divided into two components: residual stress and pressure stress. Therefore, the output voltage of the pressure sensor is derived from (12) as follows:

$$\frac{V_{out}(T)}{V_{in}} = V_{offset}(T) + \frac{1}{2}\pi_{44}(N_0, 300K)P(N, T)\left(\sigma_l^R - \sigma_t^R + \sigma_l^P - \sigma_t^P\right). \tag{15}$$

This analysis shows that the temperature affects two main factors contributing to the sensor output, namely, the piezoresistive coefficient and the residual stress. Therefore, the sensor output is a function of the pressure and temperature. The rules governing this relationship can be determined through simulation and experiment. To demonstrate the behaviors discussed above, a three-layer simulation model is designed to study the thermal stresses and deflections of thin films on a silicon substrate. The fabrication procedure for the structure depicted in Figure 4 is as follows. The silicon dioxide is deposited on a 4-inch Si wafer via LPCVD at an average fabrication temperature of 800 °C. When the final thickness of the SiO_2 is 0.6 μm, the temperature is reduced, and the aluminum layer is deposited at 150 °C to a thickness

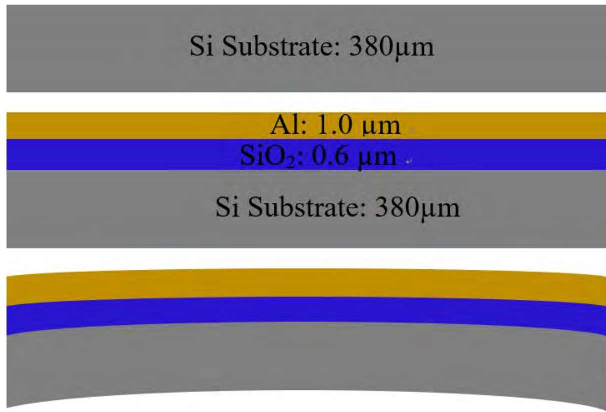

FIGURE 4. Deposition of silicon dioxide and aluminum on a wafer to validate the FEA simulation.

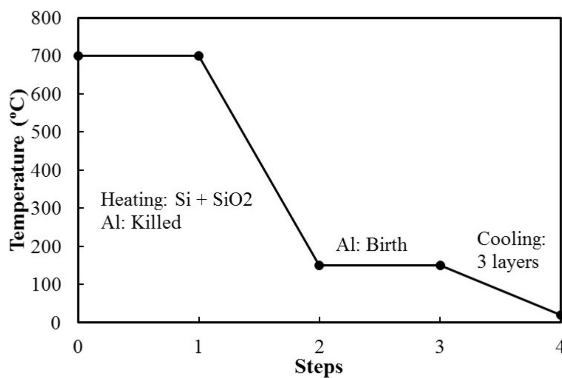

FIGURE 5. Deposition temperature profile of the silicon wafer considered in the FEA simulation.

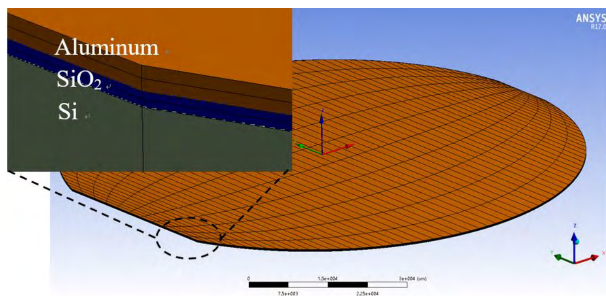

FIGURE 6. Established 3D FEA model of a silicon wafer with deposited layers.

of 1 μm. After these steps, the temperature is further reduced to 20 °C. The thermal load profile applied throughout these steps is shown in Figure 5. In addition, a 3D model of the $Si/SiO_2/Al$ structure is established, with a mesh consisting of solid 8-node brick elements. The wafer is clamped at the outside edge to provide a simple fixing point such that the circumference of the substrate is fixed in the z direction and the bottom edge is fixed in the simulation model (Figure 6).

The material properties and reference temperatures of all components used in the FEA are listed in Table 1. ANSYS is

TABLE 1. Material properties of various layers.

Material	CTE (pp/°C)	Deposition Temperature (°C)	Young's Modulus (GPa)	Poisson's Ratio
Si	3	700	170	0.25
SiO_2	0.5	700	62	0.22
Al	23.6	150	71.5	0.27
Glass	3.2	300	62	0.22

the FEA tool used to calculate the average thermal stresses. In this simulation, the birth and death technique is applied to the model in Workbench to represent the thin-film deposition. The simulation process is performed as follows:

1) The Si substrate is birthed at room temperature (20 °C).
2) The Si layer is heated to 700 °C, and the SiO_2 layer is deposited (the elements of the SiO_2 layer are birthed).
3) The Si and SiO_2 layers are cooled to 150 °C, the elements of the aluminum layer are birthed, and the Al layer is deposited.
4) When step 3 is complete, the structure is cooled to 20 °C. The residual stresses at the piezoresistor locations can be extracted to complete the analysis.

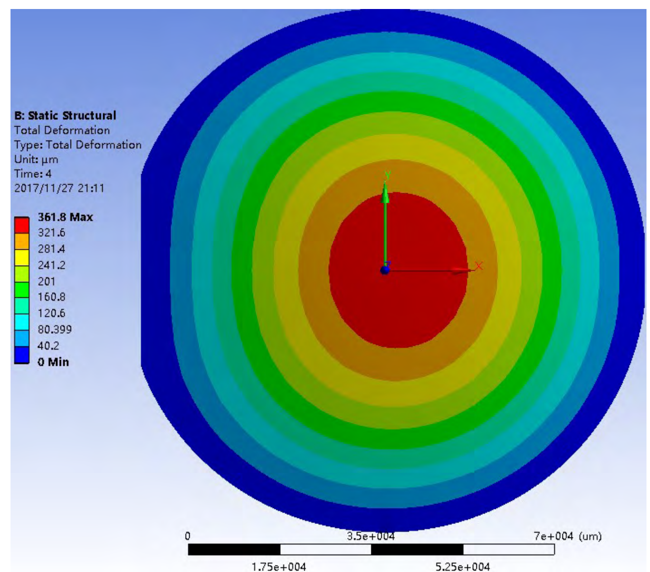

FIGURE 7. Total deformation of the wafer.

The deflection along the z-axis after the deposition of the SiO_2 and Al layers is shown in Figure 7, where the section forms an upward concavity with a maximum deflection of 361.8 μm at the center of the wafer. Moreover, Figure 8 shows the normal stress distributions oriented along the x- and y-axes. The stress on the x-axis varies from −9.85 MPa to 19.89 MPa, while that on the y-axis varies from −10.2 MPa to 22.59 MPa from the bottom of the substrate to the thin-film layers. These results show that the residual stress in the fabricated sensor can be calculated via FEA. Thus, this methodology can be used to predict the thermal hysteresis voltage shift.

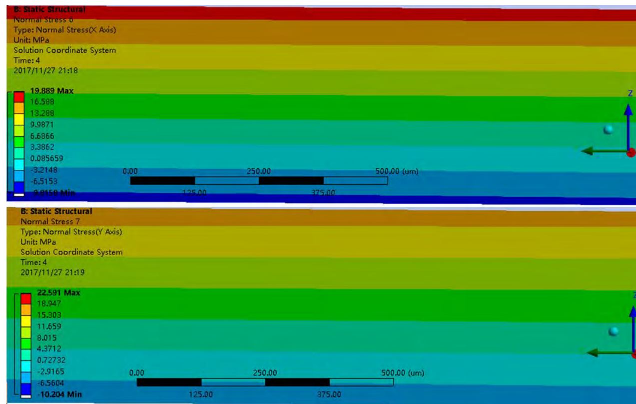

FIGURE 8. Normal stress distributions of the wafer along the x- and y-axes.

C. RESIDUAL STRESS DUE TO ANODIC BONDING

Anodic bonding is a wafer bonding process that is used to seal glass to silicon without introducing an intermediate layer. In contrast to other sealing techniques, anodic bonding involves heating and applying an electrical field to the bonding pair. The apparatus used for anodic bonding includes a hot plate, which is heated to the sealing temperature of 300 to 600 °C. The bonding parts are placed on the hotplate, and a high voltage between 200 and 2000 V is applied [26]. FEA is used to analyze the influence of the anodic-bonding-induced residual stress on the performance of the piezoresistive pressure sensor. The stress after heat is applied to the silicon membrane is obtained, and the offset voltage induced by the residual stress on the resistor is calculated using (4). Figure 9 shows one quarter of the finite element model of the packaged pressure sensor. The anodic bonding surface is located on the silicon membrane, and Pyrex 7740 glass is sealed to the cavity of the sensor. The materials used in the simulation are listed in Table 1. The bonding temperature is set to 300 °C, 400 °C or 500 °C as the reference temperature. After anodic bonding, all parts are cooled to room temperature (20 °C) with a room air convection coefficient of 110 W/m^2 °C.

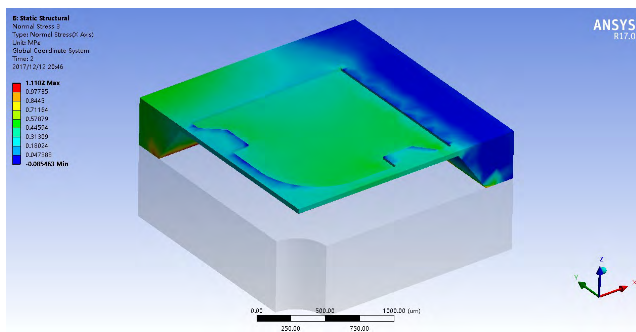

FIGURE 9. Stress distribution of the sensor.

Figure 10 shows the residual stress distributions along the sensor membrane at different bonding temperatures.

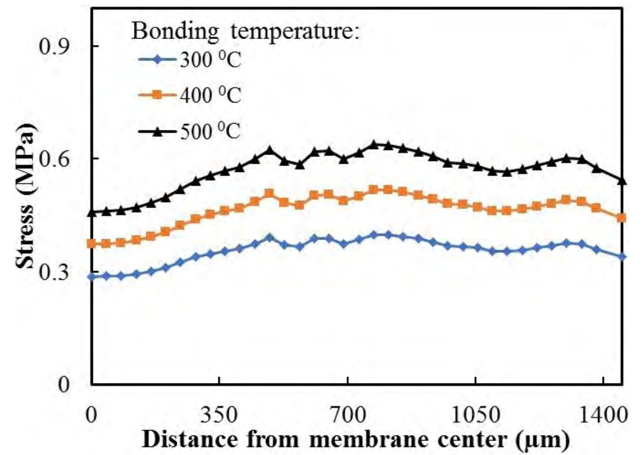

FIGURE 10. Anodic-bonding-induced residual stress distribution along the center line of the membrane.

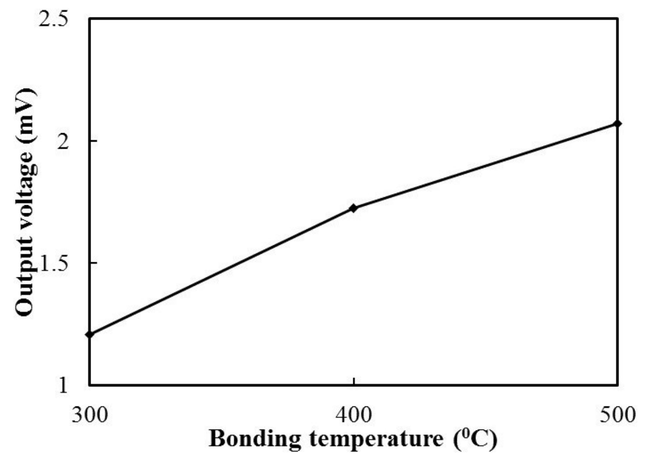

FIGURE 11. Output voltage versus the bonding temperature.

The magnitude of the induced stress increases with increasing bonding temperature. When the bonding temperature is 300 °C, without any pressure load on the membrane, the residual stress at the resistor location is approximately 0.35 MPa. As shown in Figure 11, the calculated output voltage is approximately 1.2 mV. When the bonding temperature is increased to 500 °C, the offset voltage increases to 2 mV. Thus, the bonding stress should be considered to improve the accuracy of the piezoresistive pressure sensor. In this work, a bonding temperature of 300 °C is selected for anodic bonding.

IV. FABRICATED SENSORS AND EXPERIMENTS

A. EXPERIMENTAL SETUP

After each fabricated sensor chip is separated from the silicon wafer, the back side of the sensor is attached to Pyrex 7740 glass. Hence, the chips to be used for measurement are selected from the center of the wafer surface, as illustrated in Figure 12. Each fabricated pressure sensor is simply packaged for experimental testing, with the sensor die mounted on

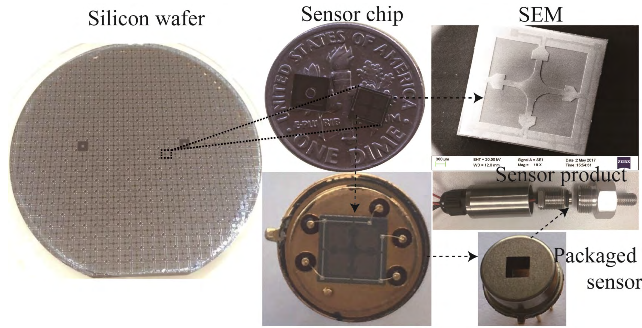

FIGURE 12. Fabricated sensor chip and packaged sensor.

a metal base. A metal shell is used to protect the sensor chip, and the tested sensor is mounted on a special fixed-screw part of the structure.

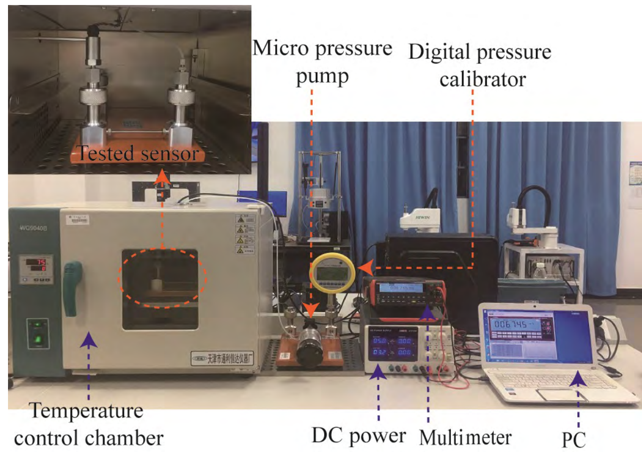

FIGURE 13. Setup for the thermal experiments.

The thermal experimental setup is shown in Figure 13. The sensor is placed in the temperature chamber, and the sensor and reference sensor are mounted in the output pressure ports of the micro pressure pump. The pressure applied to the sensor chip is controlled from 0 to 5 kPa with the micro pressure pump, and a reference pressure sensor is used along with a precision digital pressure calibrator to calibrate the tested sensor. A constant voltage bias of 5 V is applied to the Wheatstone bridge with DC power. At different pressure loads, the output of the sensor is measured using a digital multimeter.

B. RESULTS AND DISCUSSIONS

First, to demonstrate the thermal stability of the proposed sensor, measurements of the output voltage of the sensor within the range of 20 to 100 °C with zero pressure loading are presented. An expression for the measured output voltage $V_{offset}(T)$ at temperature T is obtained via the polynomial fitting method (16). The R-squared value of this equation is 0.992; note that a value closer to 1 indicates a better fit.

$$V_{offset}(T) = -0.0006T^2 + 0.0417T + 7.008 \quad (16)$$

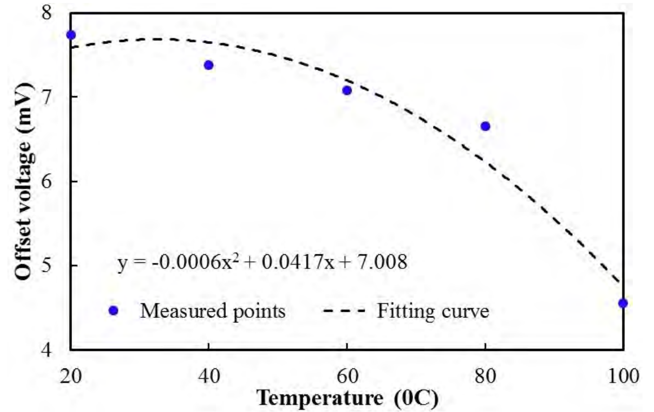

FIGURE 14. Characteristics of the temperature drift of the sensor.

Figure 14 shows the effect of temperature on the offset voltage. In this graph, each data point corresponds to data recorded over an interval of one hour. The results indicate that the zero-offset voltage is sensitive to temperature. The variation in the output offset decreases with increasing temperature; this behavior is attributed to the temperature dependence of the resistances and piezoresistive coefficient and the effects of the residual stresses generated during the fabrication and packaging processes.

Second, to validate the thermal drift of the sensor when subjected to pressure loading on the membrane in a variable-temperature environment, the results of a series of experiments performed according to the following steps are reported.

1) Set the temperature to 20 °C using the temperature control chamber.
2) Apply increasing pressure from 0 to 5 kPa in steps of 1 kPa and measure the output for 120 seconds at each pressure value.
3) Decrease the pressure in steps of 1 kPa and similarly measure the output to complete the first cycle.
4) Repeat step (2) to start the second cycle. The measurements at each temperature point must be performed over multiple cycles. Each cycle consists of a forward excursion and a reverse excursion. The average output voltage of the pressure sensor at each temperature point is then calculated.
5) Repeat steps (1) to (4) while varying the temperature from 20 to 100 °C in steps of 20 °C. The results are summarized in Table 2.

TABLE 2. Output voltage of the pressure sensor.

Pressure (kPa)	20 °C	40 °C	60 °C	80 °C	100 °C
0	7.74	7.38	7.08	6.66	4.56
1	33.24	31.62	30.66	29.28	28.23
2	58.97	57.38	55.49	54.11	52.13
3	84.69	82.02	80.31	78.06	75.81
4	110.02	108.01	105.7	103.03	100
5	135.62	132.05	129.68	126.14	122.87

The method of least squares is used to determine the linear best fit to the data in Table 2 at each temperature. The output voltage is a function of the variable pressure P at each tested temperature T_i, and the fitting results yield the following set of equations.

$$T_0 = 20\,^{\circ}\mathrm{C} : V_0(P) = 7.768 + 25.68P - 0.0196P^2$$
$$T_1 = 40\,^{\circ}\mathrm{C} : V_1(P) = 7.089 + 25.07P - 0.00143P^2$$
$$T_2 = 60\,^{\circ}\mathrm{C} : V_2(P) = 6.767 + 24.28P + 0.075P^2$$
$$T_3 = 80\,^{\circ}\mathrm{C} : V_3(P) = 6.207 + 23.81P + 0.0537P^2$$
$$T_4 = 100\,^{\circ}\mathrm{C} : V_4(P) = 4.44 + 23.98P - 0.0507P^2$$

Finally, Newton interpolation is used to find the relationship between the sensor output voltage and the temperature. The output voltage curve at the normal temperature is regarded as the baseline. MATLAB is used to generate the interpolated polynomial from the output voltage functions obtained at the various temperatures. The fitting results are as follows:

$$V_{out}(T, P) = 8.156 - 0.01595T + 25.97P - 0.0001732T^2 - 0.02349TP + 0.01154P^2 \quad (17)$$

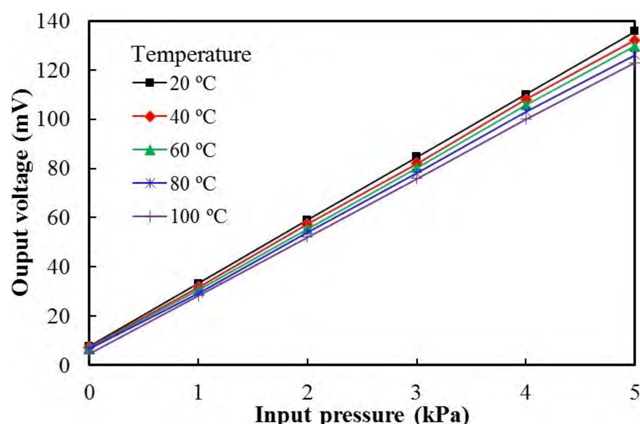

FIGURE 15. Sensor input-output curves at different temperatures.

Figure 15 shows the sensor sensitivity versus temperature. The results indicate that the output voltage increases as the temperature decreases. Therefore, the temperature influences the piezoresistive coefficient and the resistances of the resistors. The higher the temperature is, the smaller the piezoresistive effect and sensor sensitivity will be. Therefore, a temperature compensation method should be considered to reduce the temperature drift. Equation (17) can also be used to perform temperature compensation for the sensor.

V. CONCLUSION

In this study, the effect of temperature on the output of a piezoresistive sensor has been investigated through analysis of the influence of temperature on the resistances and residual stresses in the device. It can be concluded that the thermal performance instability of piezoresistive pressure sensors is mainly attributable to the effects of temperature on the piezoresistive coefficient and resistances, the residual stress due to fabrication and the residual stress due to packaging. Theoretical analysis indicates that the resistances vary with temperature and that the piezoresistive coefficient is a function of the temperature and doping level. Simulation results also show that residual stresses form in the sensor chip due to the deposition of the passivation layers and anodic bonding. The results show that the thickness of the deposited passivation layers and the fabrication temperature should be considered to reduce the residual stresses on the sensor chip. In addition, the residual stresses directly depend on the width of the glass base and the anodic bonding temperature. To validate these analyses, piezoresistive pressure sensors were fabricated, and a series of experiments were conducted at different temperatures. The experimental results show that for the tested sensor design, the offset voltage is 7.74 mV at 20 °C, and it decreases with increasing temperature. In addition, the output voltage is a function of both the temperature and the pressure load. The results indicate that temperature and residual stress conditions should be considered to improve the performance of piezoresistive pressure sensors.

REFERENCES

[1] S. Chen, M. Q. Zhu, B. H. Ma, and W. Z. Yuan, "Design and optimization of a micro piezoresistive pressure sensor," in *Proc. 3rd IEEE Int. Conf. Nano/Micro Engineered Molecular Syst.*, Jan. 2008, pp. 351–356. doi: 10.1109/NEMS.2008.4484350.

[2] T. Chen, L. Chen, L. Sun, and X. Li, "Design and fabrication of a four-arm-structure MEMS gripper," *IEEE Trans. Ind. Electron.*, vol. 56, no. 4, pp. 996–1004, Apr. 2009.

[3] G. Panzani, F. Östman, and C. Onder, "Engine knock margin estimation using in-cylinder pressure measurements," *IEEE/ASME Trans. Mechatron.*, vol. 22, no. 1, pp. 301–311, Feb. 2016.

[4] J. Hurault, S. Kouidri, and F. Bakir, "Experimental investigations on the wall pressure measurement on the blade of axial flow fans," *Experim. Thermal Fluid Sci.*, vol. 40, pp. 9–37, Jul. 2012.

[5] Y. Guo and *et al.*, "Stand-alone stretchable absolute pressure sensing system for industrial applications," *IEEE Trans. Ind. Electron.*, vol. 64, no. 11, pp. 8739–8746, Nov. 2017.

[6] R. N. DeanJr. and A. Luque, "Applications of microelectromechanical systems in industrial processes and services," *IEEE Trans. Ind. Electron.*, vol. 56, no. 4, pp. 913–925, Apr. 2009.

[7] P. Dario, M. C. Carrozza, B. Allotta, and E. Guglielmelli, "Micromechatronics in medicine," *IEEE/ASME Trans. Mechatron.*, vol. 1, no. 2, pp. 137–148, Jun. 1996.

[8] M. Messina, J. Njuguna, V. Dariol, C. Pace, and G. Angeletti, "Design and simulation of a novel biomechanic piezoresistive sensor with silicon nanowires," *IEEE/ASME Trans. Mechatron.*, vol. 18, no. 3, pp. 1201–1210, Jun. 2013.

[9] S. S. Kumar and B. D. Pant, "Design principles and considerations for the 'ideal' silicon piezoresistive pressure sensor: A focused review," *Microsyst. Technol.*, vol. 20, no. 7, pp. 1213–1247, Jul. 2014.

[10] L. Wang, "Differential structure realization in piezoresistive sensor by designing electrode configurations," *IEEE/ASME Trans. Mechatron.*, vol. 21, no. 3, pp. 1428–1433, Jun. 2016.

[11] B. Zhu, X. Zhang, Y. Zhang, and F. Sergej, "Design of diaphragm structure for piezoresistive pressure sensor using topology optimization," *Structural Multidisciplinary Optim.*, vol. 55, no. 1, pp. 317–329, Jan. 2016.

[12] T.-L. Chou, C.-H. Chu, C.-T. Lin, and K.-N. Chiang, "Sensitivity analysis of packaging effect of silicon-based piezoresistive pressure sensor," *Sens. Actuators A, Phys.*, vol. 152, pp. 29–38, May 2009.

[13] Y. Kanda and Y. Kanda, "A graphical representation of the piezoresistance coefficients in silicon," *IEEE Trans. Electron Devices*, vol. 29, no. 1, pp. 64–70, Jan. 1982.

[14] A. Boukabache and R. Pons, "Doping effects on thermal behaviour of silicon resistor," *Electron. Lett.*, vol. 38, no. 7, pp. 342–343, Mar. 2002.
[15] M. Aryafar, M. Hamedi, and M. M. Ganjeh, "A novel temperature compensated piezoresistive pressure sensor," *Measurement*, vol. 63, pp. 25–29, Mar. 2015.
[16] Y. Liu and *et al.*, "Thermal-performance instability in piezoresistive sensors: Inducement and improvement," *Sensors*, vol. 16, no. 2, p. 1984, 2016.
[17] J. A. Chiou and S. Chen, "Thermal hysteresis analysis of MEMS pressure sensors," *J. Microelectromech. Syst.*, vol. 14, no. 4, pp. 782–787, Aug. 2005.
[18] H. N. Chiang, T. L. Chou, C. T. Lin, and K. N. Chiang, "Investigation of the hysteresis phenomenon of a silicon-based piezoresistive pressure sensor," in *Proc. Int. Microsyst., Packag., Assem. Circuits Technol.*, Oct. 2007, pp. 165–168. doi: 10.1109/IMPACT.2007.4433592.[Online].
[19] R. H. Krondorfer and Y. K. Kim, "Packaging effect on MEMS pressure sensor performance," *IEEE Trans. Compon. Packag. Technol.*, vol. 30, no. 2, pp. 285–293, Jun. 2007.
[20] J. A. Chiou and S. Chen, "Thermal hysteresis and voltage shift analysis for differential pressure sensors," *Sens. Actuators A, Phys.*, vol. 135, no. 1, pp. 107–112, Mar. 2007.
[21] A. V. Tran, B. Zhu, and X. Zhang, "The development of a new piezoresistive pressure sensor for low pressures," *IEEE Trans. Ind. Electron.*, vol. 65, no. 8, pp. 6487–6496, Aug. 2018.
[22] M. Bao, *Analysis and Design Principles of MEMS Devices*. Shanghai, China: Fudan Univ., 2005.
[23] W. M. Bullis, F. H. Brewer, C. D. Kolstad, and L. J. Swartzendruber, "Temperature coefficient of resistivity of silicon and germanium near room temperature," *Solid-State Electron.*, vol. 11, no. 7, pp. 639–646, Jul. 1968.
[24] K. Chen, *MEMS/NEMS: Handbook Techniques and Applications*. New York, NY, USA: Springer, 2006.
[25] C. H. Hsueh, C. R. Luttrell, and T. Cui, "Thermal stress analyses of multilayered films on substrates and cantilever beams for micro sensors and actuators," *J. Micromech. Microeng.*, vol. 16, no. 11, p. 2509, Oct. 2006.
[26] K. Chen, *Encyclopedia of Microfluidics and Nanofluidics*. New York, NY, USA: Springer, 2008.

ANH VANG TRAN received the Ph.D. degree in micro-electro-mechanical systems (MEMS) from the South China University of Technology, in 2018. He is currently with the South China University of Technology and Le Quy Don Technical University, Hanoi, Vietnam. His research interests include the MEMS, microsensors, and intelligent manufacturing systems.

XIANMIN ZHANG received the Ph.D. degree in mechanical engineering from Beihang University, in 1993. He is currently with the South China University of Technology, as a Professor. He is currently the Dean of the School of Mechanical and Automotive Engineering, South China University of Technology, and the Director of the Guangdong Key Laboratory of Precision Equipment and Manufacturing Technology. His research interests include MEMS, precision equipment, compliant mechanisms, and advanced manufacturing.

BENLIANG ZHU received the Ph.D. degree in mechanical engineering from the South China University of Technology, in 2014, where he is currently with the South China University of Technology, as a Lecturer. His research interests include MEMS techniques, precision positioning, and manipulation at the micro- and nanoscales.